JGR Oceans

RESEARCH ARTICLE
10.1029/2019JC015727

Transport of Oil Droplets in the Upper Ocean: Impact of the Eddy Diffusivity

Michel Boufadel[1], Ruixue Liu[1], Lin Zhao[2], Youyu Lu[3], Tamay Özgökmen[4], Timothy Nedwed[2], and Kenneth Lee[3]

[1]Center for Natural Resources, The New Jersey Institute of Technology, Newark, NJ, USA, [2]Upstream Research Company, ExxonMobil, Houston, TX, USA, [3]Fisheries and Oceans Canada, Bedford Institute of Oceanography, Dartmouth, Nova Scotia, Canada, [4]Department of Ocean Sciences, Rosenstiel School of Marine and Atmospheric Sciences, University of Miami, Coral Gables, FL, USA

Key Points:
- The oil droplet distribution at the ocean surface is proportional to the rise velocity and inversely proportional to the eddy diffusivity
- The KPP model provides smaller concentrations at the water surface compared to uniform K. The impact of wave roughness was considered
- A dimensionless formulation was provided to generalize the results

Correspondence to:
M. Boufadel,
boufadel@gmail.com

Citation:
Boufadel, M., Liu, R., Zhao, L., Lu, Y., Özgökmen, T., Nedwed, T., & Lee, K. (2020). Transport of oil droplets in the upper ocean: Impact of the eddy diffusivity. *Journal of Geophysical Research: Oceans*, *125*, e2019JC015727. https://doi.org/10.1029/2019JC015727

Received 11 OCT 2019
Accepted 19 JAN 2020
Accepted article online 3 FEB 2020

Abstract The transport of oil droplets following a surface oil spill was investigated using a uniform vertical eddy diffusivity model and the K-profile parameterization model, which assumes a maximum K value at 1/3 depth of the mixed layer. The initial droplet size distribution was obtained based on the Delvigne and Sweeney (1988, https://doi.org/10.1007/s13131-013-0364-7) model. Using a uniform eddy diffusivity K_{ave}, an exact analytical solution was used to produce the transient and steady state profile of the concentration of droplets of all sizes. It was found that the concentration at the surface is proportional to the droplet rise velocity and inversely proportional to K_{ave}. Thus, small droplets (smaller than 100 μm) do not persist at the water surface. It was found that K-profile parameterization produces smaller concentrations at the water surface than the uniform K model. The impact of waves was introduced into the K-profile parameterization model through a roughness height, z_o, that is comparable to the wave height. The investigation herein reveals that the Delvigne and Sweeney approach, commonly used in oil spill modeling, is not sufficient to predict the oil droplet size distribution, and that one needs to use a vertical eddy diffusivity to accurately predict the transport in the following hours and days. A new dimensionless formulation was provided to generalize the results, and showed that transport depends on three major parameters, the water friction speed, the mixed layer depth, and the droplet diameter.

Plain Language Summary Oil slicks at sea form oil droplets that get transported into the water column based on their size (buoyancy) and the vertical mixing at sea, as governed by the eddy diffusivity (K) profile. We explored using a uniform K and the well-known K-profile parameterization model. The uniform K profile provided fundamental relations between the size of each droplet and the level of turbulence. It was found that the concentration of a given oil droplet size is proportional to the rise velocity and inversely proportional to K. Based on the Stokes' laws, the concentration at the sea surface is proportional to the square of the droplet diameter. Therefore, the concentration of 5-μm droplets (for example) is 100 times smaller than the concentration of 50-μm droplets. The K-profile parameterization model was found incapable of transporting droplets below the surface due to turbulence, which is not realistic; hence, a parameter is applied to the amended model to account for the impact of waves. A dimensionless formulation was introduced and it shows that two sea systems of various wind speeds, mixed layer depth, and droplet size could be equivalent. Therefore, one could use it to design experiments and/or to interpret sea observations.

1. Introduction

Predicting the transport of oil droplets in the water column is of major importance to assess the impact of oil spill on the ecosystem and communities (NRC, 2013). For oil released at the water surface, the long-term (hours to days) transport of oil droplets is not well understood, but the "rule of thumb" is that small oil droplets (e.g., smaller than 100 μm) do not persist at the water surface (Lunel, 1993).

Delvigne and Sweeney (DS; Delvigne & Sweeney, 1988) conducted a series of experiments to predict the droplet size distribution following a wave breakup. Their interest was on small time scales (up to tens of minutes) following droplet formation. They obtained an empirical relation of the form:

$$N(d) = a \times d^{-b} \tag{1}$$

where N(d) is the number (or number concentration) of oil droplets of diameter "d," and "a" and "b" are

constants. The constant a is directly related to the amount of oil placed at the water surface prior to wave breaking. The values of a and b are 0.067e − 6 and 2.3, respectively. The value of a depends on the volume of oil they added into their setup, and is thus not of major physical importance. We note below how future works compared to this observation.

The oil droplet size distribution (DSD) in the water immediately below the water surface depends on two mechanisms: (1) the generation of droplets at/near the water surface and (2) the vertical transport of oil droplets due to impinging waves. At the microscopic scale, an oil is created when the forces of "destruction" around it (namely due to turbulence and shear due to waves) become larger than the forces that tend to keep the droplet together (namely, oil-water interfacial tension and oil viscosity). This is well captured by the Weber number (Hinze, 1955) viz,

$$W_e = \frac{\rho u^2 d}{\sigma} \tag{2}$$

where ρ is the water density, u is a velocity due to waves, d is the droplet diameter, and σ is the oil water interfacial tension. When destructive forces increase (more turbulent flow) and/or when the IFT decreases (due to the usage of dispersant), the Weber number increases, and when it exceeds a threshold (depending on the flow geometry), the droplet would break. The impact of oil viscosity is captured using the so-called modified Weber number (Hinze, 1955), which was well developed in later works (Calabrese et al., 1986; Wang & Calabrese, 1986). The concept was introduced to the field of oil spill by Johansen et al. (2013) for oil from jets and later to oil dispersion due to waves by Johansen et al. (2015). The latter produces the d50 (volume mean diameter) of oil droplets based on wave properties and the DSD was assumed to be lognormal, with a width that would need to be estimated experimentally. Lehr et al. (2014) provided a review on the application of the Weber number for oil dispersion due to waves, and explored various forms of the modified Weber number. These approaches assume the shape of the oil DSD. Zhao et al. (2014) developed the VDROP model that can produce the oil droplet size distribution based on the hydrodynamics and oil properties, and used it to predict the theoretical oil DSD in a sea state when wave breaking occurs at the same location every 2 min. However, they did not predict the downward movement of the oil droplets in the water column, and thus, direct comparison to DS could not be made.

The transport of oil droplets (second mechanism above) was conducted in various works. Earlier were focused on the horizontal transport near the water surface (Elliot et al., 1986), In that work, the oil plume shape was described as a comet, as it had a large mass in the front followed by a "tail" representing decreasing concentrations of droplets. The behavior is due to the large buoyancy of large droplets combined with the Stokes drift, which is largest near the water surface. The behavior was reproduced in the works of the Boufadel group dealing with regular waves (Boufadel et al., 2006; Boufadel et al., 2007). Geng et al. (2016) extended the work to consider transport due to irregular waves generated based on the JONSWAP wave spectrum (Hasselmann, 1973). These studies observed that buoyant droplets would persist at depths inversely proportional to their buoyancy, and thus, neutrally buoyant droplets would spread indefinitely in the water column. However, they did not establish a clear relation between the buoyancy force, eddy diffusivity, and the orbital motion of waves. Recent works are combining computational fluid dynamics modeling and oil droplet transport; Golshan et al. (2018) investigated the transport of droplets under regular waves by combining $k - \varepsilon$ turbulence model with the Lagrangian particle tracking model NEMO3D. Cui et al. (2018) extended that work to consider a plunging breaker, and noted that the vertical motion of air pockets entrains the droplet into the water column.

Li et al. (2017) conducted plunging breaker experiments similar to those of DS, but extended the scenarios to include the impact of dispersant. They measured the DSD using high-resolution cameras and confirmed the general expression of equation (1) up to droplets with diameter of 800 μm in the absence of dispersant. In the presence of dispersant, they found b ≈ 2.2 (i.e., the decrease with an increase in the diameter is slower than obtained by DS) up to a diameter equal around 70 μm, and found b ≈ 5 for larger diameters. The correlation of DS (equation (1)) was also revisited by Johansen et al. (2015) who provided a more physical basis for equation 1, based on the Weber number, the ratio of destructive forces (due to wave height) to resistance forces (due to the oil IFT and viscosity). Other formulations, based partially on the Johansen et al. (2015) work, have been also presented (Li et al., 2017; Pan et al., 2017; Zeinstra-Helfrich et al., 2015).

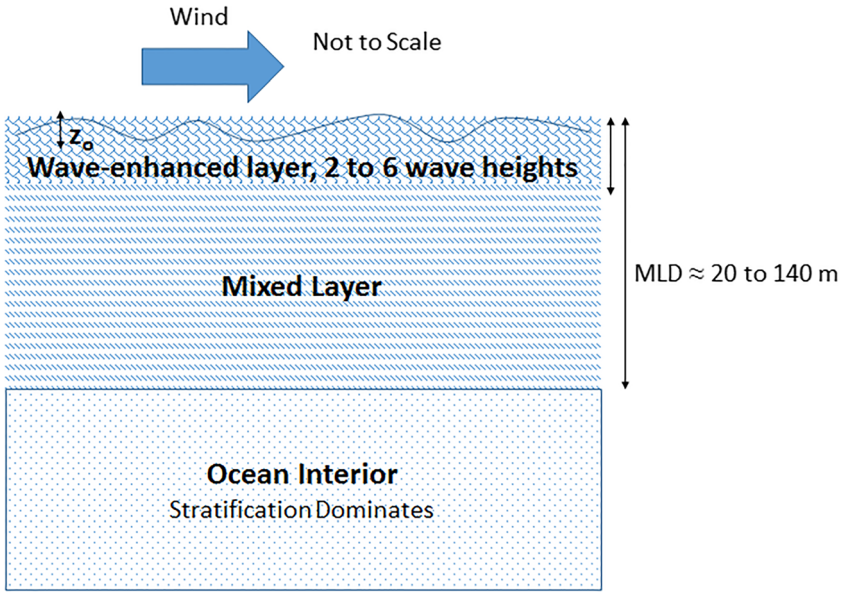

Figure 1. General definitions of sea parameters used in this paper. The roughness height z_o and the wave-enhanced layer are based on Craig and Banner (1994). The mixed layer and ocean interior, as reported in Large et al. (1994).

Given the initial DSD following a wave breakup, one may use an approach similar to that of Geng et al. (2016) to predict downward and horizontal transport. But that would require time resolutions on the order of seconds (the wave period), which is very demanding computationally. For this reason, one uses horizontally averaged quantities, such as the vertical eddy diffusivity to address only the net vertical transport. Existing works have used a depth-invariant vertical diffusion coefficient (French-McCay et al., 2008; French-McCay et al., 2017), whose value was estimated by fitting to observation. We argue herein that a more physically based approach would be to use depth-varying eddy diffusivity that can capture the impact of wind speed and waves on the transport, an approach that is rarely addressed, with the exception of recent works (Beegle-Krause et al., 2017; Boufadel et al., 2018; Nordam et al., 2019). Therefore, the goal of this work is to provide a holistic conceptual modeling of oil droplet vertical transport due to eddy diffusivity. The work attempts to use physically based arguments and measurable quantities to predict the transport of oil droplets.

At depths below the breaker zone (say one to two wave heights; Mackay et al., 1984), the kinematics of waves decrease, which is due largely to the exponential decrease of velocity with depth (Dean & Dalrymple, 1991). However, the turbulence due to waves persist for depths comparable to multiple wave heights (Drennan et al., 1992; Drennan et al., 1996; Terray et al., 1996) due to diffusion from the surface layer. Craig and Banner (1994) argued that the depth of the so-called wave-enhanced layer is around four to six wave heights (Figure 1). Beneath that, and still within the so-called mixed layer (Figure 1), measurements have shown that the "law of the wall" applies with correction due to the Coriolis force. Below the mixed layer depth (MLD), the hydrodynamics tend to be independent on the local atmospheric forcing and to depend on the internal ocean waves, shear generation, and buoyancy fluxes (due to salinity or temperature gradients). Therefore, it is reasonable to focus the investigation of surface releases to depths within the MLD.

A general approach to model the vertical (i.e., one-dimensional) migration of oil droplets of size d in the MLD is by assuming that the two mechanisms for transport are the rise velocity due to buoyancy and turbulent diffusion. This is done by ignoring transient hydraulics and droplet inertia addressed. In theoretical works on waves (Bakhoday-Paskyabi, 2015; Eames, 2008), the terminal rise velocity of droplets of diameter d w_d is given, for example, by

$$w_d = \frac{4}{3}\frac{g}{C_D}\frac{d(\rho_w - \rho_o)}{\rho_w} \text{ with } C_D = \frac{24}{\mathrm{R}_{e,d}} + \frac{3}{\sqrt{\mathrm{R}_{e,d}}} + 0.34 \tag{3a}$$

where ρ_w and ρ_o are the density of water and oil, respectively, and ν_w is the kinematic viscosity of water. The term $\mathrm{R}_{e,d} = \frac{w_d d}{\nu_w}$ is the droplet Reynolds number, reflecting the hydrodynamics around the droplet (i.e., it is

independent of the Reynolds number of the system, which impacts also the value of eddy diffusivity K, discussed next). Note that the solution of equation (3a) to obtain the velocity w_d is implicit, and thus, w_d would need to be determined by iteration. When the Reynolds number is such that $R_{e,d} = \frac{w_d d}{\nu_w} \leq 1$ (i.e., the flow around the droplet is laminar), equation (3a) becomes the well-known Stokes law (White, 1991), where the rise velocity w_d is proportional to the square of the droplet diameter, viz

$$w_d = \frac{(\rho_w - \rho_o) g d^2}{18 \rho_w \nu_w} \tag{3b}$$

Equation (3b) was presented herein as oil droplets smaller than 150 μm tend to be in the $R_{e,d} < 1$.

The concentration $c_d(z,t)$ for each size d is obtained based on the solution of the one-dimensional (vertical) advection diffusion equation, viz

$$\frac{\partial c_d}{\partial t} = \frac{\partial}{\partial z}\left(K \frac{\partial c_d}{\partial z}\right) - \frac{\partial}{\partial z}(w_d . c_d) \tag{4}$$

The dependence of the concentration on "z" and "t" is not shown in equation (4) for compactness of presentation. The term K is known as the eddy diffusivity and is discussed later. The Lagrangian form of equation (4) is (Boufadel et al., 2018)

$$Z_d = \left(w_d + \frac{dK}{dz} + \frac{R\sqrt{2Kdt}}{dt}\right)\Delta t \tag{5}$$

where R is a random number from a Gaussian distribution with mean of zero and a variance of 1.0; Z_d is the location (depth) of particle d. The gradient of the diffusivity (second term on the RHS of equation (5)) represents pseudo advection due to the spatial variation of K, and leads to a flux of material from the low-diffusivity regions to the high-diffusivity regions (Boufadel et al., 2018; Golshan et al., 2018; Röhrs et al., 2018; Visser, 1997). Neglecting the gradient would overestimate the concentration of oil droplets at the water surface, overpredicting, for example, the exposure to birds and mammals at the water surface. Equation (5) is implemented within the Lagrangian particle tracking model NEMO3D (Cui et al., 2018).

Our approach is to consider an initial "instantaneous" release of oil droplets into the water column, and to use equation (4) or (5) to track its evolution with depth and time. We will use equations (4) and (5) interchangeably—in fact, we will show that they provide the same information.

2. Eddy Diffusivity

The eddy diffusivity K has received considerable attention in the physical oceanography literature starting from the seminal work of Okubo (1971). However, at a more basic level, the eddy diffusivity may be derived based on dimensional analysis associated with boundary layer dynamics (Marusic et al., 2013; Townsend, 1980):

$$K = \kappa l u'_{rms} \tag{6}$$

where $\kappa = 0.4$ is the von Karman constant, "l" is a characteristic length scale of turbulence, and the term u_{rms} is the root mean square of turbulence velocity (turbulence fluctuations). Various works in physical oceanography investigated the range of l and u'_{rms} to obtain K. One of the most commonly used models is the K-profile parameterization (KPP) model (Large et al., 1994), in which the flux of material due to turbulent diffusion is given by the following expression:

$$F = -K\left(\frac{\partial c}{\partial z} - \gamma\right) \tag{7}$$

where c is the concentration (or any passive scalar such as number of droplets). The parameter γ is a "gain" parameter, and represents a convective flux superimposed on the diffusive flux. Equation (7) indicates that the vertical flux of material is dependent not only on the gradient of concentration but also on large-hydrodynamics processes. This is appealing from a theoretical point of view, as turbulence itself is

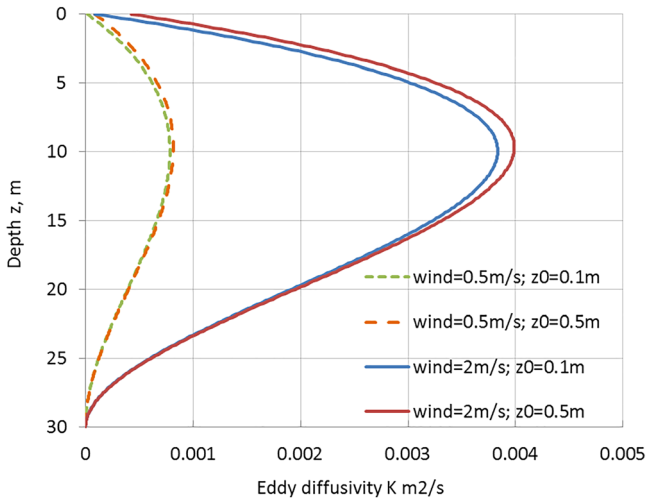

Figure 2. Eddy diffusivity profile at wind speed = 0.5 and 2 m/s and two roughness heights z_0 = 0.1 and 0.5 m (equation (8)).

nonlocal. But as our interest herein is in the one-dimensional vertical transport (i.e., averaged over the horizontal), the addition of $\gamma \neq 0$ in the equation would simply result in a uniform vertical advection that would not alter the generality of the results. For this reason, we set the gain parameter $\gamma = 0$ in equation (7).

The eddy diffusivity profile in the KPP model was stipulated based on studies in the atmospheric boundary layer to have a convex shape as function of elevation above the sea level (Troen & Mahrt, 1986). Large et al. (1994) adopted a third-order polynomial as function of water depth, which resulted in

$$K = \left(\frac{\kappa u_*}{\phi}\theta\right) z\left(1-\frac{z}{MLD}\right)^2 \tag{8}$$

where u_* is the water friction velocity, ϕ is the "stability function" in the Monin-Obukov theory for boundary layer (Monin & Yalgom, 1975), and is around 0.9. The term MLD is the mixed layer depth representing the maximum extent of the boundary layer formed due to interaction with the atmosphere. At larger depths, one reaches the "interior" of the ocean, which is dominated by stratification. The term θ is an "enhancement factor" that depends on Langmuir circulation (LC), and is equal to 1.0 when Langmuir cells are negligible, as considered here. The impact of LC on the evaluation of KPP was addressed in various works: In a rather theoretical publication, McWilliams and Sullivan (2000) discussed the incorporation of LC in the evaluation of θ, and demonstrated that θ depends inversely on the Langmuir number:

$$La = \sqrt{\frac{u^*}{U_s}} \tag{9}$$

where U_s is the Stokes drift at the surface. Typical values of La are between 0.2 and 0.7, when the LC are negligible, $La \to \infty$, in such a case, $\theta \to 1$. The impact of Langmuir cells on transport has been conducted in numerous works; Yang et al. (2014) evaluated the impact of LC on the inhibition of underwater oil jets. Reichl et al. (2016) conducted LES simulations and evaluated the impact of Lagrangian Langmuir currents in comparison to the traditional approach of using Eulerian Langmuir currents. They also estimated θ demonstrated that their approach significantly improves the prediction of upper ocean currents and temperatures. Simecek-Beatty and Lehr (2017) evaluated the impact of Langmuir circulations on the surface spreading of oil and devised a formula to account for the reduction of oil slick areas dependent on the Langmuir cells.

The dependence of K on the water friction velocity (equation (8)) reflects the conservation of shear stress at the water surface, and the fact that the input of turbulence to the ocean is proportional to u_*^3 (Terray et al., 1996). Equation (8) indicates that K increases with depth until reaching a maximum at z/MLD = 1/3, and then decreases gradually afterward to reach the value 0 at z = MLD (Figure 2).

The general shape of K has been noted also in estuaries (Visser, 1997) and in ocean flow under ice (McPhee & Smith, 1976), and it can be interpreted using equation (6) as follows. As one moves away from the boundary (surface or stratified layer beneath the mixed layer), the distance l increases as it represents the size of energetic eddies, which increase in size as one moves away from the boundary. At the same time, the turbulence velocity u'_{rms} is more or less constant initially, but it decreases at larger distances from the boundaries, because the eddies lose kinetic energy due to friction. The decrease in u'_{rms} and the increase in l result in a maximum value of K occurring in the domain, followed by a decrease.

The original authors of the KPP model (i.e., McWilliams and colleagues; Large et al., 1994) stated that the KPP model captures very well large-scale transport of momentum and passive scalars below the wave layer (a few wave height depth; Craig & Banner, 1994). This might be sufficient when dealing with water temperature or salinity. However, there is need for a higher resolution when dealing with oil spills, as the fate of oil

greatly depends on whether the oil is floating on the water surface and thus evaporates (Lee et al., 2015; NRC, 2003) or whether it is 1.0 m below the surface and thus dissolves and biodegrades (Lee et al., 2015; Prince et al., 2017; Socolofsky et al., 2019).

Turbulence just below the water surface comes primarily from shear stress due to wind (Drennan et al., 1996) and from wave breaking (Kitaigorodskii, 1983; Terray et al., 1996). However, recent works are pointing out two additional sources: nonbreaking waves and the Stokes drift shear. Babanin and Haus (2015) argued that nonbreaking waves inject turbulence into the water column, and they quantified the level of turbulence using a Reynolds number that is based on the wave height. They supported their argument by noting that turbulence in the water column have been affected by nonbreaking waves, which indicates that these waves are not irrotational as commonly assumed. Their concepts were used by Golshan et al. (2018) who modeled the transport of oil droplets due to regular waves using the k-ε model within Reynolds Averaged Navier-Stokes equations, and found a K profile that resembles that of Figure 2.

Sinha et al. (2015) conducted detailed Large-Eddy Simulation of LC and pointed out that the variation of the Stokes drift with depth generates additional turbulence that has not been accounted before. Based on their results, they amended the eddy diffusivity expression to

$$K_{wave} = K\left(1 + \gamma_s \frac{dU_s}{dz}\right) \tag{10}$$

where K is given by equation (8) and γ_s is a positive parameter on the order of MLD/u_* near the water surface (see Sinha et al., 2015, Figure 18). As $\frac{dU_s}{dz}$ is positive, the interaction of Stokes drift with LC increases the value of the eddy diffusivity, and the increase is largest at the water surface. Note also that based on equation (10), the functional form of K as function of z changes due to the dependence of $\frac{dU_s}{dz}$ on depth z.

Unfortunately, even with the usage of the most sophisticated approaches mentioned above, the value of K at the water surface remains K(0) = 0, and thus, oil droplets at the water surface can never move downward by turbulent diffusion, which is not realistic. However, based on the boundary layer theory, as one approaches the boundary, the length l in equation (6) or z in equation (8) reach a constant value equal to the roughness scale of turbulence "z_o" (Townsend, 1980). The value of z_o could represent the surface roughness due to regular waves (i.e., comparable to wave height) or it could represent a wave-enhanced layer as posited by Craig and Banner (1994). As the value is not well determined at this moment, we explored various values in this manuscript. Thus, with the addition of wave roughness, equation (10) becomes

$$K = \left(\frac{\kappa u_*}{\phi}\theta\right)(z + z_o)\left(1 - \frac{z}{MLD}\right)^2 \tag{11}$$

In equation (11), when z = 0, K takes the value $K(z=0) = \left(\frac{\kappa.u_*}{\phi}\theta\right).z_o$, a nonzero value allowing downward transport of materials from the water surface. This is shown in Figure 2.

3. Uniform Diffusivity

It is worth investigating situations where K is taken as uniform with depth. This would allow a better illustration of the physics and because uniform values have been used in the literature (French-McCay et al., 2008; Paris et al., 2012). For a uniform diffusivity and uniform water properties (density and viscosity), the evolution of the concentration of droplets of size d, c_d, is obtained by a particular form of equation (4):

$$\frac{\partial c_d}{\partial t} = K\frac{\partial^2 c_d}{\partial z^2} - w_d\frac{\partial c_d}{\partial z} \tag{12}$$

Initial condition:

$$c_d(z,0) = \begin{cases} c_{d,ini} & 0<z<z_{\text{ini}} \\ c_{\text{d,below}} & z>z_{ini} \end{cases} \tag{13}$$

where the term "ini" indicates "initial."

Boundary conditions:

At the water surface, we assume that the total flux of oil is equal to zero (i.e., the oil does not cross the water surface):

$$-K\frac{\partial c_d}{\partial z} + w_d c_d(z,t)|_{z=0} = 0 \tag{14a}$$

At infinite depth (i.e., at a large distance from the surface, such as at the MLD), we assume that the gradient of concentration is zero, which means that droplets leave the bottom domain by advection (if it occurs) but not by diffusion.

$$\frac{\partial c_d(\infty,t)}{\partial z} = 0 \tag{14b}$$

The solution to equation (12) subject to equations (13) and 14 is Van Genuchten (1982):

$$c_d(z,t) = c_{d,below} + (c_{d,ini} - c_{d,below})F_1(z,t) - c_{d,ini}F_2(z,t) \tag{15}$$

where

$$\begin{aligned} F_1(z,t) = {} & \frac{1}{2}erfc\left[\frac{(z-z_{ini})-(-w_d)t}{2(Kt)^{0.5}}\right] + (-w_d)\left(\frac{t}{\pi K}\right)^{0.5}\exp\left[\frac{(-w_d)z}{K} - \frac{(z+z_{ini}+(-w_d)t)^2}{4Kt}\right] \\ & -\frac{1}{2}\left(1+\frac{(-w_d)(z+z_{ini})}{K}+\frac{w_d^2 t}{K}\right)\exp\left(\frac{(-w_d).z}{K}\right)erfc\left[\frac{z+z_{ini}+(-w_d)t}{2(Kt)^{0.5}}\right] \end{aligned} \tag{16a}$$

$$\begin{aligned} F_2(z,t) = {} & \frac{1}{2}erfc\left[\frac{z-(-w_d)t}{2(Kt)^{0.5}}\right] + (-w_d)\left(\frac{t}{\pi K}\right)^{0.5}\exp\left[-\frac{(z-(-w_d)t)^2}{4Kt}\right] \\ & -\frac{1}{2}\left(1+\frac{(-w_d)z}{K}+\frac{w^2 t}{K}\right)\exp\left(\frac{(-w_d)z}{K}\right)erfc\left[\frac{z+(-w_d)t}{2(Kt)^{0.5}}\right] \end{aligned} \tag{16b}$$

The w_d term here is the absolute value of the rise velocity, and the negative sign placed in front of it reflects that z is positive downward.

4. Results

4.1. Results of Uniform Diffusivity

We present first the uniform K case followed by the cases where K is based on the KPP model. In addition, we will assume that the initial concentration $c_{d,below}$(below z_{ini}) is equal to zero.

4.1.1. Steady State

Although our main interest is the transient droplet distribution in the water column, it is of interest to consider first the steady state results.

The steady state solution of the uniform K case is obtained by making "t" tend to infinity. Thus, in equation 16, one sets

$$\begin{aligned} & c_d(z,t\to\infty) = c_{d,ini}{}^*(F_1(z=0,t\to\infty) - F_2(z=0,t\to\infty)) \\ & = c_{d,0}\left(\frac{w.z_{ini}}{K}\right)\exp\left(-\frac{w_d z}{K}\right) = c_{d,0}z_{ini}\left(\frac{w_d}{K}\right)\exp\left(-\frac{w_d z}{K}\right) = M_d\left(\frac{w_d}{K}\right)\exp\left(-\frac{w_d z}{K}\right) \end{aligned} \tag{17}$$

where it was recognized that the quantity $c_{d,ini}.\ z_{ini}$ is equal to the mass M_d of droplets of size d placed in the system (per unit horizontal surface area).

Equation (17) indicates that the concentration of size d at steady state (i.e., after a long time of release) is proportional to the initial mass of these droplets in the water column, M_d. (Evidently, we assume herein that no

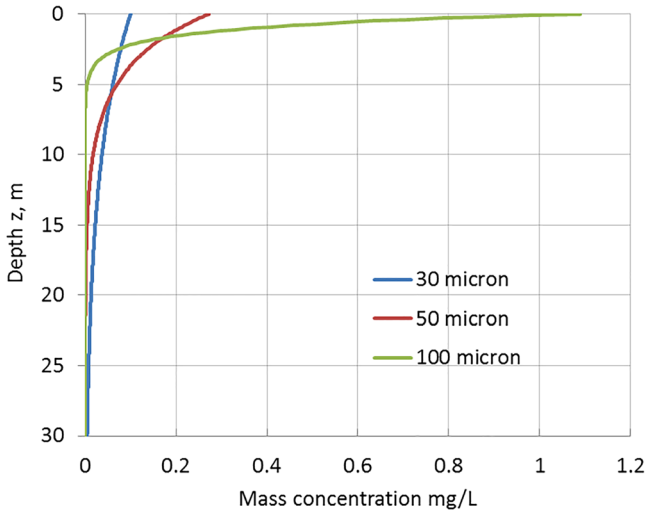

Figure 3. The mass concentration of 30-, 50-, and 100-μm droplets at steady state having each the same total mass.

coalescence and breakup of oil droplets occur.) This means that for the steady state result, the depth z_{ini} is not important, rather the mass of droplets of a given size.

Assuming $K = 5.11 \times 10^{-4} m^2/s$ and $M_d = 1.0$ for all droplet sizes, and using equation (3b) to compute the rise velocity based on an oil density of 887.0 kg/m^3, water density of 998.0 kg/m^3, and water viscosity of $1.08 \times 10^{-3} Pa \cdot s$, we plotted the steady state solutions (equation (17)) in Figure 4,3 for diameters of size 30, 50, and 100 μm.

Figure 3 reflects the fact that the concentration decreases exponentially with depth with a "decay" constant equal to $\frac{w_d}{K}$. Thus, the concentration of larger droplets decreases fastest with depth. At the water surface (i.e., z = 0), equation (17) gives

$$c_d(z=0, t\to\infty) = M_d \frac{w_d}{K} = c_{d,ini} z_{ini} \frac{w_d}{K} \tag{18}$$

Thus, all concentrations are inversely proportional to the eddy diffusivity, and the concentration of each size is proportional to the rise velocity of droplets of that size. In particular, neutrally buoyant particles (i.e., $w_d = 0$) do not persist at the water surface at steady state (i.e., after a long a time).

4.2. The DS Correlation as Initial Condition

Taking the initial mass equal for all droplets was adopted in the previous section to illustrate the physics of the problem. In reality, an expedient (and physically justifiable) means for estimating the initial concentration (mg/L) of each droplet size is through the DS correlation (equation (1)). The concentration (mass of oil per unit volume of water) can be obtained by multiplying the number concentration of equation (1) by the oil density (assumed to be the same for all droplets) and the volume of the corresponding droplets. This leads to

$$c_{ini,d} = a d^{-b} \rho_o \frac{\pi d^3}{6} = \frac{a \rho_o \pi d^{3-b}}{6} \tag{19}$$

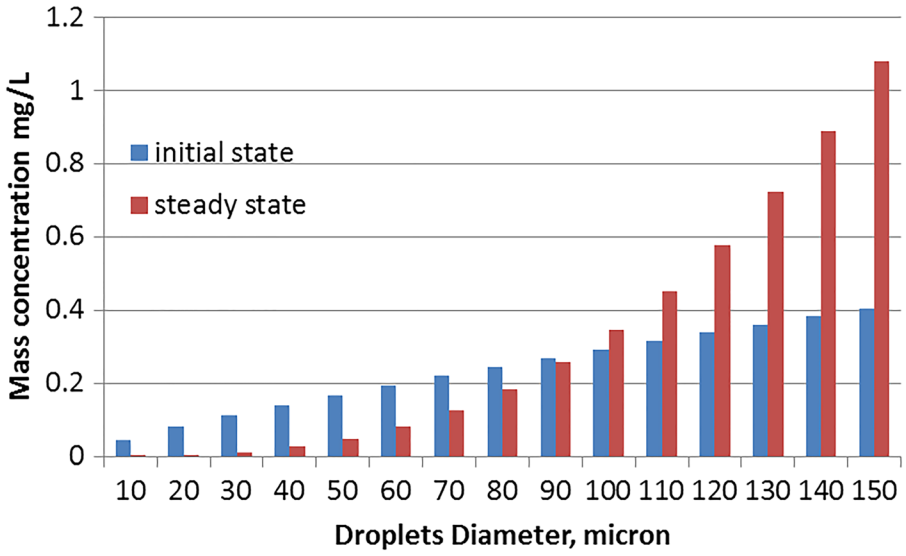

Figure 4. Mass fraction at the surface at the initial time based on DS correlation (equation (19)) and at steady state (based on equation (21)).

Table 1
Simulation Scenarios of Transient Concentration

Droplet diameter (μm)	Rise velocity (m/s)	Wind speed (m/s)	Friction velocity u_* (m/s)	K_{ave} (m^2/s; equation (22))
30	5.04×10^{-5}	0.5	3.94×10^{-4}	4.43×10^{-4}
30	5.04×10^{-5}	2	1.90×10^{-3}	2.20×10^{-3}
100	5.60×10^{-4}	0.5	3.94×10^{-4}	4.43×10^{-4}
100	5.60×10^{-4}	2	1.90×10^{-3}	2.20×10^{-3}

Equation (19) indicates that the initial concentration of droplets of size d varies at the power of (3 − b) of the diameter. As $b \approx 2.2$, the initial concentration is proportional to $d^{0.8} \approx d$. Thus, the DS correlation provides concentrations that increase almost linearly with the droplet diameter. For example, the concentration of 100-μm droplets is approximately 10 times the concentration of the 10-μm droplets. This can be noted in Figure 3 for a = 1.0 (the value of a show no difference in calculating concentration values) and z_{ini} = 1 m.

Using equation (17), the steady state profile in the water column for droplets of size d is given by

$$c_d(z, t\to\infty) = c_{d,ini}\left(\frac{w_d.z_{ini}}{K}\right)\exp\left(-\frac{w_d.z}{K}\right) = \frac{a\rho_o\pi z_{ini}(\rho_w-\rho_o)g}{108\mu K}d^{2.8}\exp\left(-\frac{w_d z}{K}\right) \quad (20)$$

And at the surface, the concentration of droplets of size d is

$$c_d(z=0, t\to\infty) = \frac{a\rho_o\pi z_{ini}(\rho_w-\rho_o)g}{108\mu K}\times d^{2.8} \quad (21)$$

The steady state mass concentrations (equation (21)) for the 10 to 150 μm at the surface are shown in Figure 4.

One notes in Figure 4 that the oil mass at the surface decreases with respect to the initial value for diameters smaller than 90 μm and the converse occurs for larger diameters. This could be interpreted based on the following argument. At the surface, the concentration at steady state is (equation (21)) $c(z=0, t\to\infty) = c_{d,ini}\frac{w_d z_{ini}}{K}$. Therefore, when the quantity $\frac{w_d z_{ini}}{K}$(which is a Peclet number) is larger than 1.0, the concentration will increase from the initial value $c_{d,ini}$. Otherwise, the concentration of droplet will decrease. Combining equation (21) with the expression for the terminal velocity (equation 3), one obtains that for $\frac{w_d z_{ini}}{K} > 1, w_d = \frac{(\rho_w-\rho_o)gd^2}{18\mu} > \frac{K}{z_{ini}}$. Therefore, droplets with diameter $d_c > \sqrt{\frac{18K\mu}{\Delta\rho g z_{ini}}}$ will rise to the surface. For this simulation condition, K = 5.11×10^{-4} m^2/s and $z_{ini} = 1$ m resulting in $d_c = 92$ μm, in agreement with Figure 4.

The mass concentration at steady state reflects the fact that the concentration at steady state is proportional to the rise velocity w_d, which by equation (3b) is proportional to the square of the droplet diameter, meaning that the steady state concentration of, for example, 125-μm droplets is 100 times that of 12.5-μm droplets.

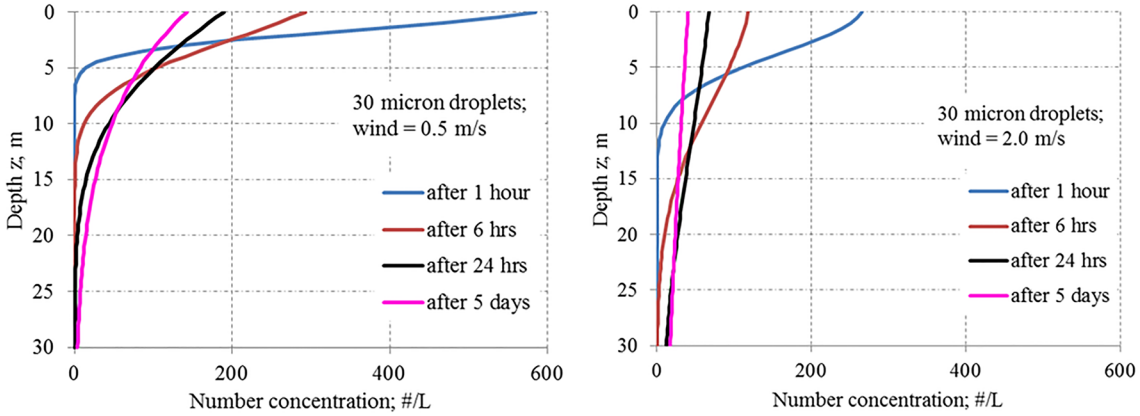

Figure 5. Number concentration of 30-μm droplets based on uniform K distribution under (a) wind speed = 0.5 m/s and (b) wind speed = 2 m/s.

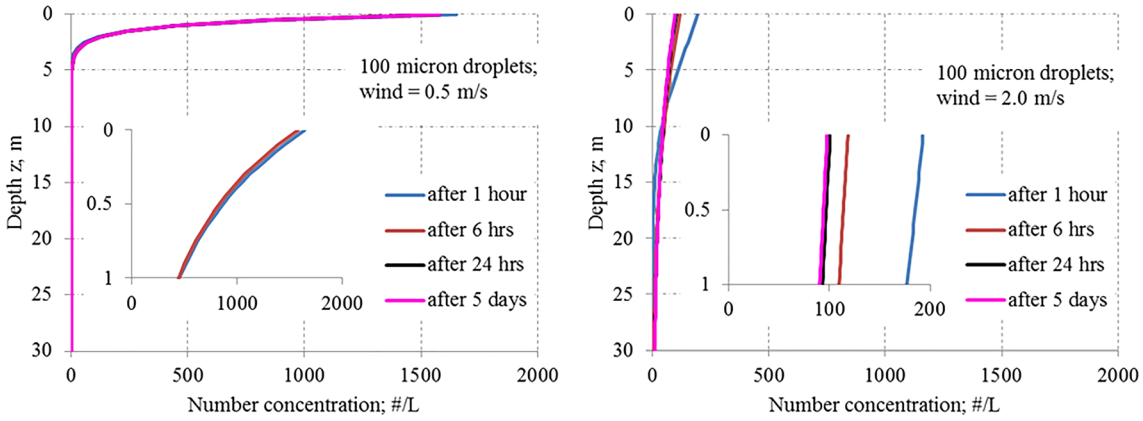

Figure 6. Number concentration of 100-μm droplets based on uniform K distribution under (a) wind speed = 0.5 m/s and (b) wind speed = 2 m/s (Table 1).

5. Transient Simulations

As one of our goals is to compare the KPP model with the uniform K case, we selected a situation where the uniform K value to be equal to the average K based on the KPP model. Thus, the average K is obtained by taking the average of equation (11):

$$K_{ave} = \frac{1}{MLD}\int_0^{MLD} K dz = \frac{\kappa u_*}{\phi}\left(\frac{MLD}{12} + \frac{z_0}{3}\right) \tag{22}$$

where $\kappa = 0.4$ and $\phi = 0.9$. Therefore, for a given wind speed, one obtains the friction velocity u_* (Table 1), and subsequently K (equation (11)) and K_{ave} (equation (22)).

Figure 5 shows concentration profiles of 30-μm droplets as function of time for two wind speeds: 0.5 m/s (left panel) and 2.0 m/s (right panel). An increase in the wind speed increases the magnitude of K_{ave} (Table 1) and results in further penetration of droplets into the water column.

Figure 6 shows concentration profiles for the 100-μm droplets as function of time for two wind speeds: 0.5 m/s (left panel) and 2.0 m/s (right panel). An increase in the wind speed resulted in a major decrease of the concentration at the water surface (compare the left panel to the right panel). However, unlike the profile of the 30-μm droplets (Figure 5), the profiles of the 100-μm droplets do not change much over time and/or with depth. This is due to the strong role of buoyancy of the 100-μm droplets in comparison with the weak turbulence level considered herein, as wind speeds of 5 m/s and faster could easily occur at sea (discussed later).

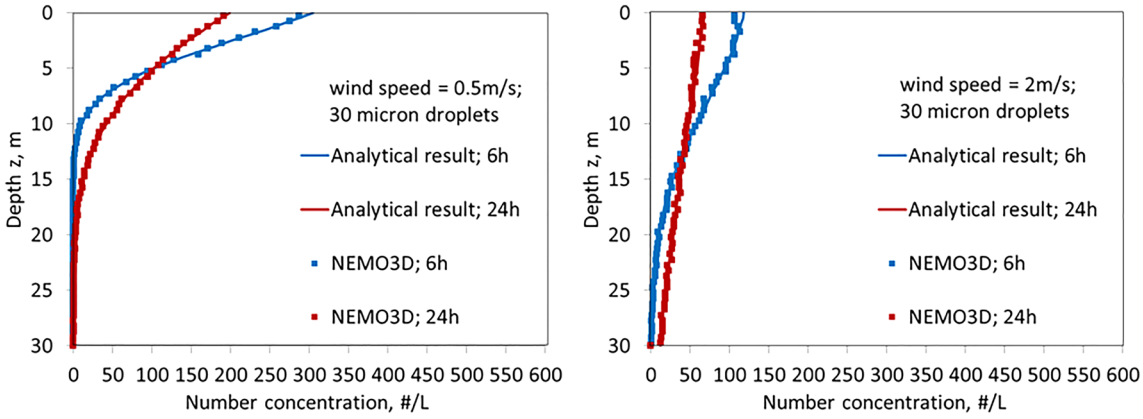

Figure 7. Profiles of number concentration of 30-μm droplets based on uniform K obtained using the analytical solution and NEMO3D (a) wind speed = 0.5 m/s and (b) wind speed = 2 m/s.

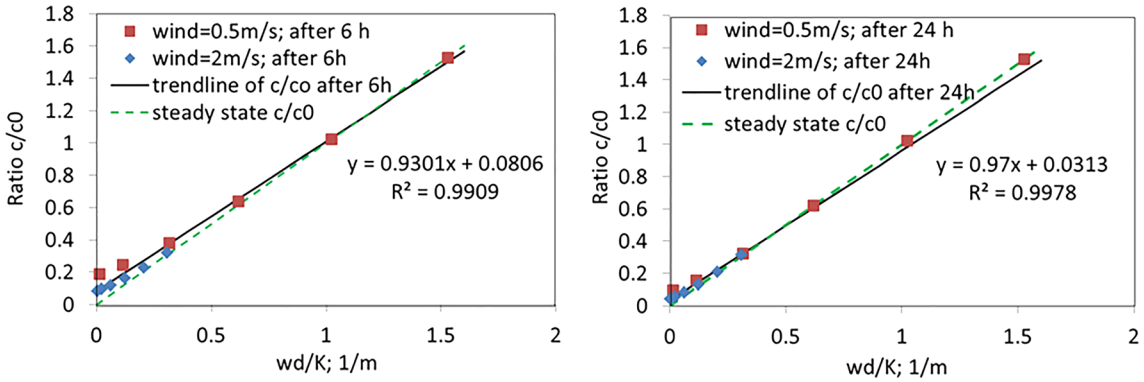

Figure 8. Surface concentration ratio to the initial concentration under two wind speeds (a) 6 hr and (b) 24 hr.

The model NEMO3D was used to predict the concentration of droplets based on equation (5) assuming a uniform K profile given by K_{ave}. Thirty realizations (simulations) were conducted. In each, a total of 2,500 droplets were placed uniformly with depth until z = 1.0 m. They were placed in two bins each of 0.5-m depth, and thus, the initial concentration was $c_{d,ini} = 1{,}250$ # /L in each bin. Figure 7 reports the comparison for 30-μm droplets for the two wind speeds 0.5 and 2.0 m/s and two arbitrary times of interest: 6 and 24 hr. Figure 7 shows that NEMO3D was able to closely reproduce the exact solution, confirming further that equations (4) and (5) are equivalent (i.e., that a Lagrangian solution for the transport reproduces the Eulerian solution). The agreement between NEMO3D and the exact analytical solution was even closer for the 100-μm droplets, and is not shown here for brevity.

The steady state solution for the uniform K profiles provides a clear connection between the droplet diameter and its persistence at the water surface. However, the time to reach steady state could be on the order of days for droplets that are 30 μm subjected to a 0.50-m/s wind, and is unlikely to be of major interest when responding to oil spills where the time frame is a few days. Therefore, it would be desirable to see whether the buoyancy and eddy diffusivity play a role at earlier times, namely, at 6 and 24 hr. For this reason, we plotted in Figure 8 the surface concentration ratio at times $t = 6$ and 24 hr as function of the rise speed divided by K for the two wind speeds (0.5 and 2.0 m/s). The relation appears linear in agreement with the steady-state situation leading to an equation of the form:

$$\frac{c_d(z=0,t)}{c_0(z=0,t=0)} = 0.93 z_{ini}\frac{w_d}{K} \quad att = 6\ hours hr \tag{23a}$$

$$\frac{c_d(z=0,t)}{c_0(z=0,t=0)} = 0.97 z_{ini}\frac{w_d}{K} \quad att = 2424 hours hr \tag{23b}$$

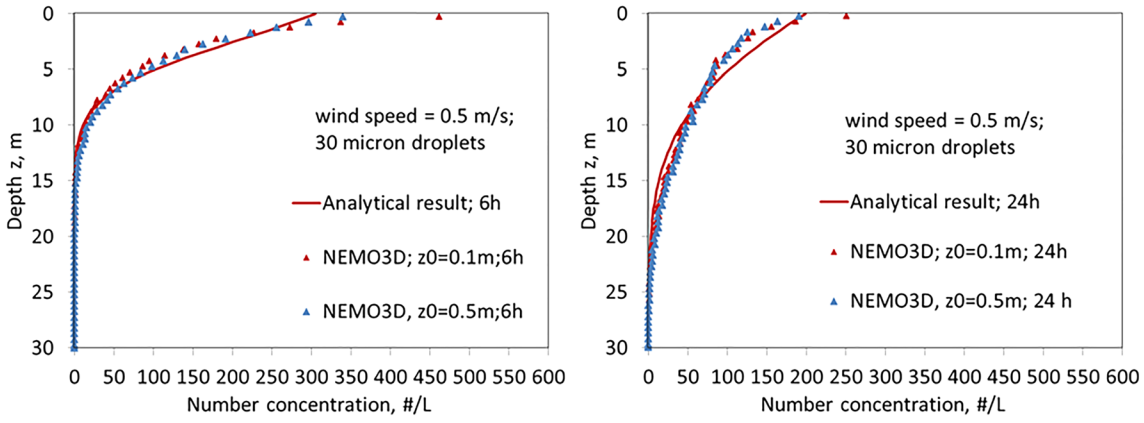

Figure 9. Wind speed 0.5 m/s and 30-μm droplets. Number concentration of the analytical results based on uniform K and NEMO3D results based on the KPP model at (a) 6 hr and (b) 24 hr.

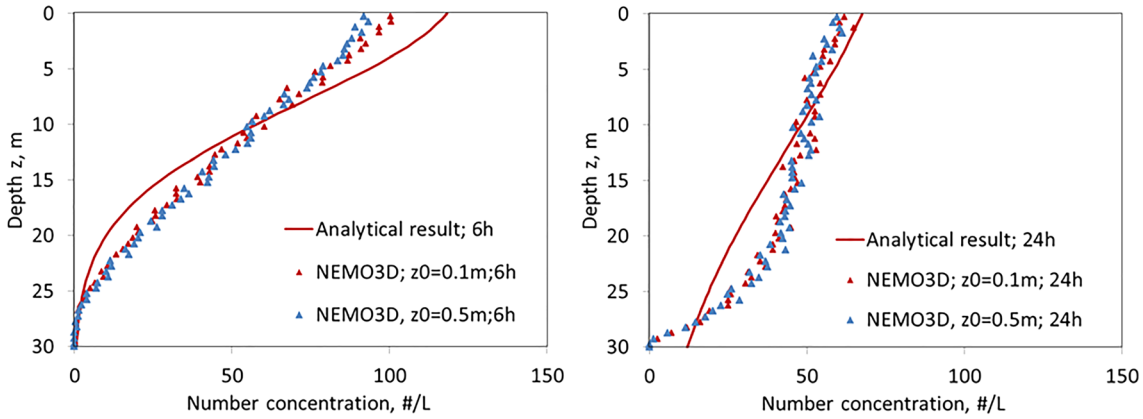

Figure 10. Wind speed 2.0 m/s and 30-μm droplets. Number concentration of analytical result based on uniform K and NEMO3D result based on the KPP model at (a) 6 hr and (b) 24 hr.

Based on Figure 8, equation 23 applies well for the wind speed of 2.0 m/s at both 6 and 24 hr, and applies well for a wind speed of 0.5 m/s at 24 hr. The deviation occurs at small rise velocities at 6 hr. Thus, in fairly general conditions (e.g., wind speed larger than 2.0 m/s), the transient concentration of a given droplet size at the water surface at 24 hr is directly proportional to its terminal rise velocity and inversely proportional to the eddy diffusivity.

The comparison between the KPP profile results and the analytical results using K_{ave} is reported in Figure 9 for 30-μm droplets at wind speed of 0.5 m/s. The impact of the surface roughness (due to waves), z_o, was investigated using two values of z_o, 0.1 and 0.5 m. Figure 9a shows that the KPP model provides concentrations smaller than the uniform K model in the top 5 m with the exception of the value at the surface, which seems to be greatly dependent on the z_o value. A value of $z_o = 0.5$ m resulted in KPP concentrations at the surface (i.e., $z = 0$) that are essentially equal to those of the uniform K (Figures 9a and 9b). At 24 hr (Figure 9b), the concentration at 10–15-m depth based on the KPP model was larger than that of the uniform K, which is likely due to the fact droplets migrated toward the maximum K value, which was at 10 m.

Figure 10 shows the KPP and uniform K results for the 30-μm droplets at a wind speed of 2.0 m/s for the two z_o values. Near the surface, the KPP model provided smaller concentrations than the uniform K model at both 6 and 24 hr, and the impact of z_o is small, only visible at 6 hr. The discrepancy at 24 hr is due to the fact that the uniform K model uses K_{ave} at $z = 30$ m, while K decreases to reach 0 at $z = 30$ m, and the K gradient (second term in equation (5)) tends to move droplets upward there. This was not observed when the wind speed was 0.5 m/s (Figure 10) because K was small in that case, and the droplets remained above $z = 20$ m.

Figures 9 and 10 show that at the water surface, the KPP model provided smaller values of the concentration in comparison with the uniform K model using the average value. The difference is generally small (less than 20%). But more importantly, the difference seems to increase rapidly with the wind speed, especially for the 30-μm droplets (left panels of Figures 8 and 9).

A wind speed of 5.0 m/s was also considered. However, we had to increase the depth of the mixed layer to MLD = 120 m as high level of turbulence resulted in major displacement of droplets to the MLD, which Figure 11 indicates that, compared to the smaller wind speed, the stronger turbulence situation will spread the droplets more into the water column for the times considered so far (6 and 24 hr), resulting in smaller concentrations. Figure 11 also shows that the difference between the uniform (analytical) eddy diffusivity model and the KPP model decreases with time (compare the 24- to the 6-hr result).

6. Dimensionless Formulation

Rewriting equation (5) where starred parameters represent dimensional quantities, one obtains

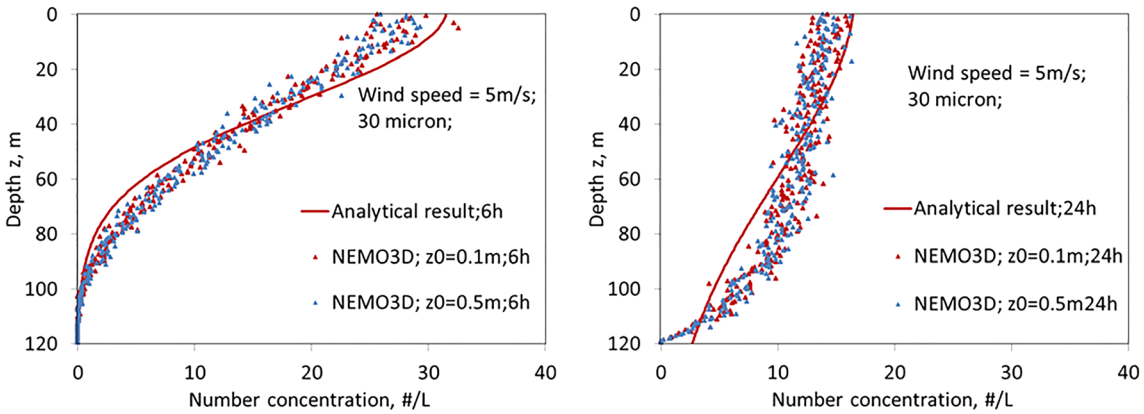

Figure 11. Wind speed 5.0 m/s for 30-μm droplets. Number concentration for analytical result based on uniform K and NEMO3D result based on KPP model at (a) 6 hr and (b) 24 hr.

$$\frac{dZ_d^*}{dt*} = w_d^* + \frac{dK^*}{dz^*} + \frac{R\sqrt{2K^*dt^*}}{dt^*} \tag{24}$$

$$z_{t+1}{}^* = z_t{}^* + w_d{}^*\Delta t^* + \frac{dK^*}{dz^*}\Delta t^* + R\sqrt{2K^*\Delta t^*} \tag{25}$$

Now let

$$z = \frac{z^*}{L_0}w_d = \frac{w_d^*}{U_0}t = \frac{t^*}{T_0}K = \frac{K^*}{K_0} \tag{26}$$

where L_o, U_o, T_o, and K_o are the characteristic length, velocity, time, and diffusivity, respectively. Let $L_0 = MLD$, $U_0 = u_*$, $T_0 = \frac{L_0}{U_0} = \frac{MLD}{u_*}$, and let $K_0 = u_*.MLD$. Then,

$$K^* = \frac{\kappa.u_*}{\phi}\left(z^* + z_o^*\right)\left(1 - \frac{z^*}{MLD}\right)^2 = \frac{\kappa MLDu_*}{\phi}(z + z_o)(1-z)^2 = K_o\frac{\kappa}{\phi}(z + z_o)(1-z)^2 = K_oK \tag{27}$$

Inserting equations (26) and (27) into equation (25), one obtains

$$\begin{aligned} z_{t+1} &= z_t + w_d\Delta t + \frac{K_o}{u_*.MLD}\frac{dK}{dz}\Delta t + \sqrt{\frac{K_o}{u_*.MLD}}\times R\sqrt{2K\Delta t} \\ z_{t+1} &= z_t + w_d\Delta t + \frac{dK}{dz}\Delta t + R\sqrt{2K\Delta t} \end{aligned} \tag{28}$$

The dimensionless nature of equation (28) and the fact that it resembles to equation (25) allows its usage for a wide range of situations, as discussed next. For example, for a given dimensionless rise velocity $w_d = \frac{w_d^*}{u_*}$, one notes that

$$w_d = \left(\frac{w_d^*}{u_*}\right)_1 = \left(\frac{w_d^*}{u_*}\right)_2 \tag{29}$$

where "1" and "2" represent different systems. Thus, the concentration profile of a small rise velocity droplet in a system with a small water friction velocity (for example, system 1) would be the same as the profile obtained from a larger droplet in a larger water friction velocity system (system 2) as long as equation (29) is satisfied. Alternatively, two systems with different wind speeds would have the same time evolution if their T_o is the same, as shown in Table 2.

Table 2
Similarity Between Two Systems Using the Dimensionless Formulation of This Study

Wind speed (m/)s	0.5	2
u^* (m/s)	3.9e−4	1.9e−3
MLD (m)	30	146
T_o (s)	77,000	77,000

Table 3
Application of the Dimensionless Formulation to Generalize the Results of One-Dimensional Simulation

Consider that based on the dimensionless formulation, C/Co = 0.385 for droplets of size w_d as reported below, at the locations and time reported below	*Location and time in a dimensional system with the properties below.* Wind speed = 0.5 m/s, u_* = 3.9e − 4 m/s; MLD = 30 m, T_o = 77,000 s	*Location and time in a dimensional system with the properties below.* Wind speed = 5.0 m/s, u_* = 5.7e − 3 m/s; MLD = 120 m, T_o = 21,000 s
w_d = 0.1	$w_d^* = w_d.u_* = 3.9e-5$ m/s, droplet diameter = 26 μm for oil density = 887 kg/m^3	$w_d^* = w_d.u_* = 5.7e-4$ m/s, droplet diameter = 100 μm for oil density = 887 kg/m^3
z = 0.7	$z^* = z.MLD = 21$ m	$z^* = z.MLD = 84$ m
t = 0.4	$t^* = t.T_o = 8.55$ hr	$t^* = t.T_o = 2.33$ hr

The judicious selection of the parameters (namely, u_* and MLD) allowed the actual value of the eddy diffusivity to cancel out resulting in an expression similar to the original (dimensional expression). Two examples are presented in Table 3. This removes the constraint of accounting for the dimensional value of the eddy diffusivity, as one notes from observing equation (28). Nevertheless, the dimensionless formulation cannot be generalized to include the DS model, as the DS model is empirical in nature, and it is for this reason that we presented the formulation herein and not earlier.

7. Conclusions

The transport of oil droplets following a surface oil spill was investigated by assuming a uniform eddy diffusivity, K, profile and a vertical profile based on the KPP model (Large et al., 1994). In the latter, K increases initially with depth to reach a maximum at one third of the MLD, and then subsequently decreases gradually. The initial droplet size distribution was assumed to be obtained based on the Delvigne and Sweeney (Delvigne & Sweeney, 1988) model, and it resulted in the mass concentration (mg/L) increasing almost linearly with the droplet diameter. The solution for the vertical transport problem (equation (4)) was obtained first using a uniform K, which provided an exact analytical solution (equation 16), where the concentration of a given droplet size at the water surface was $c_d(z=0, t\to\infty) = M_d \frac{w_d}{K_{ave}}$, where M_d is the total (initial) mass of oil of size d, w_d is the rise velocity of droplets of size d (equation (3b)), and K_{ave} is the average vertical eddy diffusivity within the mixed layer (Figure 1). This means that neutrally buoyant material would not persist at the water surface. This also means that an increase in the wind speed (Table 1) and subsequently K would result in smaller concentration at the water surface, which was observed at sea during storms. In addition, based on Stokes' law (equation (3a)), the finding indicates that the oil concentration of a given droplet size is proportional to the square of the diameter, reflecting a sharp decrease of the oil concentration with the diameter. This result could explain observations that droplets smaller than 100 μm do not persist at the water surface. The results (Figure 8) suggest that the steady state relation provided above applies closely at t = 24 hr or larger, especially at wind speeds of 2.0 m/s and larger. In particular, one has $\frac{c_d(z=0,t=24\ \mathrm{hr})}{c_{d,ini}} \sim 0.90$ to $0.97 * z_{ini} \frac{w_d}{K_{ave}}$, where $c_{d,ini}$ is the initial oil concentration occurring over a depth z_{ini}. Thus, in the absence of detailed modeling, one may use this relation to interpret the measurements at sea following a spill.

The model NEMO3D (Cui et al., 2018) was further validated in this work, and it matched very closely the exact analytical solution results for a uniform K at all times considered, including steady state. The model was then used to predict the transient concentration at t = 6 and 24 hr. It was found that the KPP produces smaller concentrations at the water surface in comparison with the assumption of a uniform K, and that the difference increases with the wind speed and the decrease in droplet diameter. The impact of waves was introduced into the KPP model through a roughness height, z_o, that is comparable to the wave height based on previous works in physical oceanography (Craig & Banner, 1994; Drennan et al., 1992). It was found that the value of z_o has essentially no impact on the concentration profiles at depth, but greatly impact the concentration within a few wave depths. As oil response depends greatly on the oil concentration at or just below the water surface, it is advisable to use the proposed new expression of K (equation (11)) when applying the KPP model.

A new dimensionless formulation was provided for the transport of oil droplets due to turbulent diffusion and buoyancy. It allowed generalization of the results of oil droplet transport. The formulation can be used with the DS model as initial condition. However, one cannot easily make the DS model (Delvigne & Sweeney,

1988) dimensionless as the model is empirical, and because the slip (or rise) velocity of oil droplets do not seem much affected by turbulence, as is the case for air bubbles (Spelt & Biesheuvel, 1997) or sediment particles (Nielsen, 1993).

The investigation herein reveals that the Delvigne and Sweeney (Delvigne & Sweeney, 1988) approach is not sufficient to predict the oil DSD in the water column, and that one needs to use a vertical eddy diffusivity to accurately the transport in the following hours and days. The resulting DSD was very different from that of DS. This work provides an effort to bridge between advances in the fields of physical oceanography and needs in the field of oil spill modeling.

Acknowledgments
This work was funded in part by the Multi Partner Research Initiative from the Department of Fisheries of Oceans Canada to the project "Transport of oil at the meter scale." This research was funded in part by The Gulf of Mexico Research Initiative. However, the article does not reflect necessarily the views of the funding agency, and no official endorsement should be implied. Data are publicly available through the Gulf of Mexico Research Initiative Information & Data Cooperative (GRIIDC) at https://data.gulfresearchinitiative.org (doi:10.7266/YFNW5W7Q).

References

Babanin, A. V., and B. K. Haus (2015), On the turbulence beneath finite amplitude water waves, *arXiv preprint arXiv:1510.05053*.
Bakhoday-Paskyabi, M. (2015). Particle motions beneath irrotational water waves. *Ocean Dynamics*, *65*(8), 1063–1078.
Beegle-Krause, C., T. Nordam, E. J. Davies, A. N. Smith, M. McPhee, L.-G. Faksness, et al. (2017), Oil droplet surfacing probabilities under realistic low turbulence in Arctic ice, paper presented at International Oil Spill Conference Proceedings, International Oil Spill Conference.
Boufadel, F., Cui, J., Katz, T. N., & Lee, K. (2018). On the transport and modeling of dispersed oil under ice. *Marine Pollution Bulletin*, *135*, 569–580. https://doi.org/10.1016/j.marpolbul.2018.07.046
Boufadel, K., Du, V. K., & Weaver, J. (2007). Lagrangian simulation of oil droplets transport due to regular waves. *Environmental Modelling & Software*, *22*(7), 978–986.
Boufadel, R., Bechtel, D., & Weaver, J. (2006). The movement of oil under non-breaking waves. *Marine pollution bulletin*, *52*(9), 1056–1065. https://doi.org/10.1016/j.marpolbul.2006.01.012
Calabrese, R. V., Chang, T. P. K., & Dang, P. T. (1986). Drop breakup in turbulent stirred-tank contactors. Part I: Effect of dispersed-phase viscosity. *AIChE Journal*, *32*, 657–666.
Craig, P. D., & Banner, M. L. (1994). Modeling wave enhanced turbulence in the ocean surface layer. *Journal of Physical Oceanography*, *24*, 2546–2559.
Cui, F., Boufadel, M. C., Geng, X., Gao, F., Zhao, L., King, T., & Lee, K. (2018). Oil droplets transport under a deep-water plunging breaker: Impact of droplet inertia. *Journal of Geophysical Research: Oceans*, *123*, 9082–9100. https://doi.org/10.1029/2018JC014495
Dean, R. G., & Dalrymple, R. A. (1991). *Water wave mechanics for engineers and scientists*. Hackensack, NJ, US:World Scientific Publishing Co Inc.
Delvigne, G. A., & Sweeney, C. (1988). Natural dispersion of oil. *Oil and Chemical Pollution*, *4*(4), 281–310. https://doi.org/10.1007/s13131-013-0364-7
Drennan, K. Kahma, E. Terray, M. Donelan, A. and S. Kitaigorodskii (1992), Observations of the enhancement of kinetic energy dissipation beneath breaking wind waves, in Breaking waves, pp. 95-101, Springer.
Drennan, M., Donelan, A., Terray, E. A., & Katsaros, K. B. (1996). Oceanic turbulence dissipation measurements in SWADE. *Journal of Physical Oceanography*, *26*, 808–815.
Eames, I. (2008). Settling of particles beneath water waves. *Journal of Physical Oceanography*, *38*(12), 2846–2853.
Elliot, A. J., Hurford, N., & Penn, C. J. (1986). Shear diffusion and the spreading of oil slicks. *Marine Pollution Bulletin*, *17*(7), 308–313.
French-McCay, D. P., C. Mueller, J. Payne, E. Terrill, M. Otero, S. Y. Kim, et al. (2008), Dispersed oil transport modeling calibrated by field-collected data measuring fluorescein dye dispersion, paper presented at International Oil Spill Conference, American Petroleum Institute.
French-McCay, D. P., Tajalli-Bakhsh, T., Jayko, K., Spaulding, M. L., & Li, Z. (2017). Validation of oil spill transport and fate modeling in Arctic ice. *Arctic Science*, *4*, 71–97.
Geng, X., Boufadel, M. C., Ozgokmen, T., King, T., Lee, K., Lu, Y., & Zhao, L. (2016). Oil droplets transport due to irregular waves: Development of large-scale spreading coefficients. *Marine Pollution Bulletin*, *104*(1), 279–289.
Golshan, R., Boufadel, M., Rodriguez, V., Geng, X., Gao, F., King, T., et al. (2018). Oil droplet transport under non-breaking waves: An Eulerian RANS approach combined with a Lagrangian particle dispersion model. *Journal of Marine Science and Engineering*, *6*(1), 7.
Hasselmann, K. (1973). Measurements of wind-wave growth and swell decay during the Joint North Sea Wave Project (JONSWAP). *Ergänzung zur Deut. Hydrogr. Z., Reihe A*, *A8*(12), 1–95.
Hinze, J. O. (1955). Fundamentals of the hydrodynamic mechanism of spliting in dispersion processes. *AICHE Journal*, *1*, 289–295.
Johansen, Ø., Brandvik, P. J., & Farooq, U. (2013). Droplet breakup in subsea oil releases: Part 2—Predictions of droplet size distributions with and without injection of chemical dispersants. *Marine Pollution Bulletin*, *73*, 327–335. https://doi.org/10.1016/j.marpolbul.2013.04.012
Johansen, Ø., Reed, M., & Bodsberg, N. R. (2015). Natural dispersion revisited. *Marine Pollution Bulletin*, *93*(1), 20–26. https://doi.org/10.1016/j.marpolbul.2015.02.026
Kitaigorodskii, S. A. (1983). On the theory of the equilibrium range in the spectrum of wind generated gravity waves. *Journal of Physical Oceanography*, *13*(5), 816–827. https://doi.org/10.1175/1520-0485(1983)013<0816:OTTOTE>2.0.CO;2
Large, W. G., McWilliams, J. C., & Doney, S. C. (1994). Oceanic vertical mixing: A review and a model with a nonlocal boundary layer parameterization. *Reviews of Geophysics*, *32*(4), 363–403.
Lee, K., Boufadel, M., Chen, B., Foght, J., Hodson, P., Swanson, S., & Venosa, A. (2015). *The behaviour and environmental impacts of crude oil released into aqueous environments*. Ottawa: The Royal Society of Canada.
Lehr, W., Simecek-beatty, D., & Michel, B. C. (2014). Review of recent studies on dispersed oil droplets distribution, paper presented at Arctic and Marine Oil Spills. *Environment Canada, Edmonton, Canada, June*, *6-8*, 2014.
Li, J., Miller, J., Wang, S. K., & Katz, J. (2017). Size distribution and dispersion of droplets generated by impingement of breaking waves on oil slicks. *Journal of Geophysical Research: Oceans*, *122*, 7938–7957. https://doi.org/10.1002/2017JC013193
Li, M., Spaulding, L., & French-McCay, D. (2017). An algorithm for modeling entrainment and naturally and chemically dispersed oil droplet size distribution under surface breaking wave conditions. *Marine Pollution Bulletin*, *119*(1), 145–152. https://doi.org/10.1016/j.marpolbul.2017.03.048

Lunel, T. (1993), Dispersion: Oil droplet size measurements at sea, paper presented at International Oil Spill Conference, American Petroleum Institute.
Mackay, D., Chau, A., Hossain, K., & Bobra, M. (1984). Measurement and prediction of the effectiveness of oil spill chemical dispersants. *Oil Spill Chemical Dispersants, Research, Experience and Recommendations, ASTM STP*, *840*, 38–54.
Marusic, I., Monty, J. P., Hultmark, M., & Smits, A. J. (2013). On the logarithmic region in wall turbulence. *Journal of Fluid Mechanics*, *716*.
McPhee, M. G., & Smith, J. D. (1976). Measurements of the turbulent boundary layer under pack ice. *Journal of Physical Oceanography*, *6*(5), 696–711.
McWilliams, J. C., & Sullivan, P. P. (2000). Vertical mixing by Langmuir circulations. *Spill Science & Technology Bulletin*, *6*(3-4), 225–237.
Monin, A. S., & Yalgom, A. M. (1975). *Statistical characteristics of wave and turbulent components of the random velocity field in the marine surface layer, in Statitical Fluid Mechanics, Mechanics of Turbulence, Pts I and II*, (p. 1260). Cambridge, MA, US: The MIT Press.
Nielsen, P. (1993). Turbulence effects on the settling of suspended particles. *Journal of Sedimentary Research*, *63*(5), 835–838.
Nordam, T., Nepstad, R., Litzler, E., & Röhrs, J. (2019). On the use of random walk schemes in oil spill modelling. *Marine pollution bulletin*, *146*, 631–638.
NRC (2003). *Oil in the sea III: inputs, fates, and effects*. Washington, D.C., PR, US: National Academies Press.
NRC (2013). *An ecosystem services approach to assessing the impacts of the deepwater horizon oil spill in the Gulf of Mexico*. Washington, D.C., PR, US: The National Academies Press.
Okubo, A. (1971). Oceanic diffusion diagrams. *Deep Sea Research and Oceanographic Abstracts*, *18*(8), 789–802. https://doi.org/10.1016/0011-7471(71)90046-5
Pan, Z., Zhao, L., Boufadel, M. C., King, T., Robinson, B., Conmy, R., & Lee, K. (2017). Impact of mixing time and energy on the dispersion effectiveness and droplets size of oil. *Chemosphere*, *166*, 246–254. https://doi.org/10.1016/j.chemosphere.2016.09.052
Paris, C. B., Hénaff, M. L., Aman, Z. M., Subramaniam, A., Helgers, J., Wang, D.-P., et al. (2012). Evolution of the Macondo well blowout: Simulating the effects of the circulation and synthetic dispersants on the subsea oil transport. *Environmental science & technology*, *46*(24), 13,293–13,302.
Prince, R. C., Butler, J. D., & Redman, A. D. (2017). The rate of crude oil biodegradation in the sea. *Environmental Science & Technology*, *51*(3), 1278–1284. https://doi.org/10.1021/acs.est.6b03207
Reichl, B. G., Wang, D., Hara, T., Ginis, I., & Kukulka, T. (2016). Langmuir turbulence parameterization in tropical cyclone conditions. *Journal of Physical Oceanography*, *46*(3), 863–886.
Röhrs, J., K.-F. Dagestad, H. Asbjørnsen, T. Nordam, J. Skancke, C. Jones, and C. Brekke (2018), The effect of vertical mixing on the horizontal drift of oil spills.
Simecek-Beatty, D., & Lehr, W. J. (2017). Extended oil spill spreading with Langmuir circulation. *Marine pollution bulletin*, *122*(1-2), 226–235. https://doi.org/10.1016/j.marpolbul.2017.06.047
Sinha, N., Tejada-Martínez, A. E., Akan, C., & Grosch, C. E. (2015). Toward a K-profile parameterization of Langmuir turbulence in shallow coastal shelves. *Journal of Physical Oceanography*, *45*(12), 2869–2895.
Socolofsky, S. A., Gros, J., North, E., Boufadel, M. C., Parkerton, T. F., & Adams, E. E. (2019). The treatment of biodegradation in models of sub-surface oil spills: A review and sensitivity study. *Marine Pollution Bulletin*, *143*, 204–219.
Spelt, P., & Biesheuvel, A. (1997). On the motion of gas bubbles in homogeneous isotropic turbulence. *Journal of Fluid Mechanics*, *336*, 221–244.
Terray, E., Donela, M., Agrawal, Y., Drennan, W., Kahma, K., Williams, A., et al. (1996). Estimates of kinetic energy dissipation under breaking waves. *Journal of Physical Oceanography*, *26*(792-807).
Townsend, A. A. (1980). *The structure of turbulent shear flow*. Cambridge, UK: Cambridge university press.
Troen, I., & Mahrt, L. (1986). A simple model of the atmospheric boundary layer; sensitivity to surface evaporation. *Boundary-Layer Meteorology*, *37*(1-2), 129–148.
Van Genuchten, M. T. (1982), Analytical solutions of the one-dimensional convective-dispersive solute transport equation, US Department of Agriculture, Agricultural Research Service.
Visser, A. W. (1997). Using random walk models to simulate the vertical distribution of particles in a turbulent water column. *Marine Ecology Progress Series*, *158*, 275–281.
Wang, C., & Calabrese, R. V. (1986). Drop breakup in turbulent stirred-tank contactors. Part II: Relative influence of viscosity and interfacial tension. *AIChE Journal*, *32*(4), 667–676.
White, F. M. (1991). *Viscous fluid flow, 1991*, (pp. 335–393). New York: MacGraw.
Yang, D., Chamecki, M., & Meneveau, C. (2014). Inhibition of oil plume dilution in Langmuir ocean circulation. *Geophysical Research Letters*, *41*, 1632–1638. https://doi.org/10.1002/2014GL059284
Zeinstra-Helfrich, M., Koops, W., & Murk, A. J. (2015). The NET effect of dispersants—A critical review of testing and modelling of surface oil dispersion. *Marine pollution bulletin*, *100*(1), 102–111.
Zhao, L., Torlapati, J., Boufadel, M. C., King, T., Robinson, B., & Lee, K. (2014). VDROP: A comprehensive model for droplet formation of oils and gases in liquids-Incorporation of the interfacial tension and droplet viscosity. *Chemical Engineering Journal*, *253*, 93–106.